J|A|C|S
ARTICLES
Published on Web 05/26/2006

Dynamics on the Microsecond Timescale in Microporous Aluminophosphate AlPO-14 as Evidenced by ^{27}Al MQMAS and STMAS NMR Spectroscopy

Sasa Antonijevic,[†] Sharon E. Ashbrook,[‡] Silke Biedasek,[§] Richard I. Walton,*[,¶] Stephen Wimperis,*[,#] and Huaixin Yang[£]

Contribution from the Institut des Sciences et Ingénierie Chimiques, Ecole Polytechnique Fédérale de Lausanne, 1015 Lausanne, Switzerland, School of Chemistry and EaStCHEM, University of St Andrews, St Andrews KY16 9ST, United Kingdom, Institut für Technische und Makromolekulare Chemie, Universität Hamburg, 20146 Hamburg, Germany, Department of Chemistry, The Open University, Milton Keynes MK7 6AA, United Kingdom, Department of Chemistry and WestCHEM, University of Glasgow, Glasgow G12 8QQ, United Kingdom, and Beijing National Laboratory for Condensed Matter Physics, Institute of Physics, Chinese Academy of Sciences, Beijing 100080, China

Received November 11, 2005; E-mail: r.i.walton@open.ac.uk; s.wimperis@chem.gla.ac.uk

Abstract: Multiple-quantum magic angle spinning (MQMAS) and satellite-transition magic angle spinning (STMAS) are two well-known techniques for obtaining high-resolution, or "isotropic", NMR spectra of quadrupolar nuclei. It has recently been shown that dynamics-driven modulation of the quadrupolar interaction on the microsecond timescale results in linewidths in isotropic STMAS spectra that are strongly broadened, while, in contrast, the isotropic MQMAS linewidths remain narrow. Here, we use this novel methodology in an ^{27}Al ($I = 5/2$) NMR study of the calcined-dehydrated aluminophosphate AlPO-14 and two forms of as-synthesized AlPO-14, one prepared with isopropylamine ($C_3H_7NH_2$) as the template molecule and one with piperidine ($C_5H_{10}NH$). For completeness, the ^{31}P and ^{13}C (both $I = 1/2$) MAS NMR spectra are also presented. A comparison of the ^{27}Al MQMAS and STMAS NMR results show that, although calcined AlPO-14 appears to have a rigid framework structure, the extent of motion in the two as-synthesized forms is significant, with clear evidence for dynamics on the microsecond timescale in the immediate environments of all four Al sites in each material. Variable-temperature ^{27}Al STMAS NMR studies of the two as-synthesized AlPO forms reveal the dynamics to be complex, with the motions of both the guest water molecules and organic template molecules shown to be contributing. The sensitivity of the STMAS NMR experiment to the presence of microsecond timescale dynamics is such that it seems likely that this methodology will prove useful in NMR studies of host−guest interactions in a wide variety of framework materials.

Introduction

The aluminophosphates (AlPOs) are an important class of microporous solid, with widespread practical applications in, for example, separation and catalysis. A number of AlPO structures are made up exclusively of corner-sharing tetrahedral units (AlO_4 and PO_4) and are thus direct analogues of aluminosilicate zeolites.[1] However, unique AlPO forms, not seen in aluminosilicate chemistry, are also found, with some arising from the possibility of aluminum occurring in five- and six-coordination sites. AlPOs are normally synthesized hydrothermally from an aqueous mixture of aluminum oxyhydroxide or alkoxide and phosphoric acid. An amine or quaternary ammonium salt is also added, and the presence of this organic "template" molecule, which is incorporated into the cavities within the structure, is essential in producing the microporous framework. The thermal stabilities of AlPOs are similar to those of zeolites, and hence calcination at 500−600 °C can be used to remove the template molecule and any occluded water.

Investigations of host−guest interactions in microporous solids are important in understanding the sorption and any catalytic properties of the materials.[2,3] However, it is often difficult to study template or adsorbed guest molecules in porous solids using standard diffraction techniques, owing to the considerable positional and/or dynamic disorder of the guest species. It is therefore necessary to turn to methods, such as solid-state magic angle spinning (MAS) NMR spectroscopy, that directly probe the local environments of individual atom types and are sensitive to dynamic behavior. In the case of AlPOs,

[†] Ecole Polytechnique Fédérale de Lausanne.
[‡] University of St Andrews.
[§] Universität Hamburg.
[¶] The Open University.
[#] University of Glasgow.
[£] Chinese Academy of Sciences.

(1) Wilson, S. T.; Lok, B. M.; Messina, C. A.; Cannan, T. R.; Flanigen, E. M. *J. Am. Chem. Soc.* **1982**, *104*, 1146.
(2) Dutta, P. K. *J. Inclusion Phenom. Mol. Recognit. Chem.* **1995**, *21*, 215.
(3) Fyfe, C. A.; Diaz, A. C.; Grondey, H.; Lewis, A. R.; Forster, H. *J. Am. Chem. Soc.* **2005**, *127*, 7543.

10.1021/ja057682g CCC: $33.50

^{27}Al and ^{31}P MAS NMR have been widely used to study the microporous framework,[4−8] while ^{13}C and ^{15}N MAS NMR have been used for the template molecules.[9−11] In addition, a variety of double- and triple-resonance NMR techniques have been used for heteronuclear correlation via *J*-couplings (yielding information on bond connectivities and hence aiding spectral assignment)[12−14] or dipole−dipole couplings (providing information on internuclear distances and hence aiding structure determination).[15−18]

^{27}Al, with spin quantum number $I = 5/2$, is a quadrupolar nucleus, and resolution in ^{27}Al MAS NMR spectra is consequently impaired by a residual anisotropic broadening arising from second-order effects of the quadrupolar interaction. The advent of the multiple-quantum (MQ) MAS technique in 1995 and of the satellite-transition (ST) MAS technique in 2000 were thus important developments for the study of AlPOs and zeolites as, by refocusing the second-order quadrupolar broadening, they allowed truly high-resolution or "isotropic" ^{27}Al spectra to be obtained using only conventional solid-state NMR equipment.[19,20] Recently, we showed, using a simple theoretical model and experimental examples drawn from ^{17}O (also spin $I = 5/2$) NMR of hydrous magnesium silicates, that dynamics-driven modulation of the quadrupolar interaction on the microsecond timescale results in linewidths in isotropic STMAS spectra that are strongly broadened, while, in contrast, the isotropic MQMAS linewidths remain narrow.[21] Comparison of isotropic MQMAS and STMAS linewidths therefore provides a very sensitive test of the presence of molecular-scale dynamics on the microsecond timescale in solids and can be used to unambiguously exclude static disorder as a source of the line-broadening.

In this paper, we apply this novel methodology in an ^{27}Al NMR study of calcined-dehydrated AlPO-14 and two forms of as-synthesized AlPO-14, one prepared with isopropylamine ($C_3H_7NH_2$) as the template molecule and one with piperidine ($C_5H_{10}NH$). For completeness, the ^{31}P and ^{13}C MAS NMR spectra will also be presented. AlPO-14 was among the first AlPOs reported by Wilson et al. in 1982[1] and has been widely studied by several NMR methods, including ^{27}Al MQMAS[22,23] and a variety of ^{27}Al−^{31}P heteronuclear correlation techniques.[13,23,24] The structure is made up of four-, six-, and eight-rings with the three-dimensional channel system delimited by the eight-rings.[25,26] We show that a comparison of isotropic ^{27}Al MQMAS and STMAS linewidths reveals the presence of dynamics on the microsecond timescale in both the as-synthesized forms of AlPO-14; however, such dynamics appear to be absent in the calcined-dehydrated form.

Experimental Details

Isopropylamine-templated AlPO-14 ("ipa-AlPO-14") was prepared using a method adapted from that of Broach et al.[25] Hydrated aluminum oxide ("pseudo-boehmite", Sasol Ltd., $Al_2O_3 \cdot 1.9H_2O$) was dispersed in deionized water by stirring. To this was added orthophosphoric acid (85% in water) followed by isopropylamine, and the mixture was stirred to give a homogeneous mixture of composition $C_3H_7NH_2$:Al_2O_3:P_2O_5:$35H_2O$. This was sealed in a Teflon-lined 45 mL autoclave and heated at 160 °C for 10 h. The white solid product was collected by suction filtration, washed with deionized water, and dried in air at 110 °C. Powder X-ray diffraction revealed the material to be phase pure, and the data were consistent with the structure elucidated by Broach et al.[25,26] Thermogravimetric analysis was also consistent with the chemical formula $Al_8P_8O_{32}(OH)_2 \cdot (C_3H_{10}N)_2(H_2O)_2$. Piperidine-templated AlPO-14 ("pip-AlPO-14") was prepared using similar method: a mixture of composition $2C_5H_{10}NH$:Al_2O_3:P_2O_5:$40H_2O$ was heated for 115 h at 200 °C under hydrothermal conditions with addition of a small amount of the first material (<30 mg) as seed crystals to avoid the presence of AlPO-17 as a byproduct. Powder X-ray diffraction data were consistent with those reported by Zibrowius et al.[27] Calcined samples of AlPO-14 were prepared by heating the as-synthesized materials in static air at 600 °C for 3 h. After packing in a MAS rotor, complete dehydration of the calcined samples was ensured by heating the open rotor at 100 °C overnight.

NMR experiments were performed on a Bruker Avance 400 spectrometer, equipped with a widebore 9.4 T magnet, operating at a Larmor frequency, ν_0, of 104.3 MHz for ^{27}Al ($I = 5/2$), 162.0 MHz for ^{31}P ($I = 1/2$), 100.6 MHz for ^{13}C ($I = 1/2$), and 400.1 MHz for ^{1}H ($I = 1/2$). Triple-quantum ($m_I = +3/2 \leftrightarrow -3/2$) MAS NMR experiments were performed using the phase-modulated split-t_1 pulse sequence shown in Figure 14b of ref 28. STMAS and DQF-STMAS[29] ($m_I = \pm 3/2 \leftrightarrow \pm 1/2$) NMR experiments were performed using the phase-modulated split-t_1 pulse sequences shown in Figure 1b of ref 30 and Figure 45a of ref 31, respectively. In a series of preliminary experiments, the temperature inside the MAS rotor was calibrated for each MAS rate using the ^{207}Pb chemical shift of $Pb(NO_3)_2$. Except where stated, spectra were recorded at ambient temperatures (~293 + 9 K for a MAS rate of 10 kHz and ~293 + 21 K for a MAS rate of 20 kHz, on account of the frictional heating). For variable-temperature ^{27}Al STMAS experiments, in particular, the spinning angle was accurately adjusted to the magic angle (54.736°) at each temperature using the ^{87}Rb ($I = 3/2$) STMAS signal from $RbNO_3$,[30] which was packed either in the same MAS rotor as the AlPO or in a separate rotor. Chemical shifts

(4) Rocha, J.; Lourenco, J. P.; Ribeiro, M. F.; Fernandez, C.; Amoureux, J. P. *Zeolites* **1997**, *19*, 156.
(5) Philippou, A.; Salehirad, F.; Luigi, D. P.; Anderson, M. W. *J. Phys. Chem. B* **1998**, *102*, 8974.
(6) Bodart, P. R.; Amoureux, J. P.; Pruski, M.; Bailly, A.; Fernandez, C. *Magn. Reson. Chem.* **1999**, *37*, S69.
(7) Marichal, C.; Vidal, L.; Delmotte, L.; Patarin, J. *Microporous Mesoporous Mater.* **2000**, *34*, 149.
(8) Roux, M.; Marichal, C.; Paillaud, J. L.; Fernandez, C.; Baerlocher, C.; Chezeau, J. M. *J. Phys. Chem. B* **2001**, *105*, 9083.
(9) Thursfield, A.; Anderson, M. W. *J. Phys. Chem.* **1996**, *100*, 6698.
(10) Thursfield, A.; Anderson, M. W.; Dwyer, J.; Hutchings, G. J.; Lee, D. *J. Chem. Soc., Faraday Trans.* **1998**, *94*, 1119.
(11) Vidal, L.; Pray, C.; Patarin, J. *Microporous Mesoporous Mater.* **2000**, *39*, 113.
(12) Massiot, D.; Fayon, F.; Alonso, B.; Trebosc, J.; Amoureux, J. P. *J. Magn. Reson.* **2003**, *164*, 160.
(13) Wiench, J. W.; Pruski, M. *Solid State Nucl. Magn. Reson.* **2004**, *26*, 51.
(14) Fyfe, C. A.; Bretherton, J. L.; Skibsted, J.; Zahei-Niaki, M. H.; Kalliaguine, S. *Stud. Surf. Sci. Catal.* **2004**, *154*, 1238.
(15) Fyfe, C. A.; Mueller, K. T.; Grondey, H.; Wong-Moon, K. C. *J. Phys. Chem.* **1993**, *97*, 13484.
(16) Fernandez, C.; Delevoye, L.; Amoureux, J. P.; Lang, D. P.; Pruski, M. *J. Am. Chem. Soc.* **1997**, *119*, 6858.
(17) Fernandez, C.; Lang, D. P.; Amoureux, J. P.; Pruski, M. *J. Am. Chem. Soc.* **1998**, *120*, 2672.
(18) Fernandez, C.; Morais, C.; Rocha, J.; Pruski, M. *Solid State Nucl. Magn. Reson.* **2002**, *21*, 61.
(19) Frydman, L.; Harwood, J. S. *J. Am. Chem. Soc.* **1995**, *117*, 5367.
(20) Gan, Z. *J. Am. Chem. Soc.* **2000**, *122*, 3242.
(21) Ashbrook, S. E.; Antonijevic, S.; Berry, A. J.; Wimperis, S. *Chem. Phys. Lett.* **2002**, *364*, 634.
(22) Fernandez, C.; Amoureux, J. P.; Chezeau, J. M.; Delmotte, L.; Kessler, H. *Microporous Mater.* **1996**, *6*, 331.
(23) Fyfe, C. A.; zu Altenschildesche, H. M.; Wong-Moon, K. C.; Grondey, H.; Chezeau, J. M. *Solid State Nucl. Magn. Reson.* **1997**, *9*, 97.
(24) Delevoye, L.; Fernandez, C.; Morais, C. M.; Amoureux, J. P.; Montouillout, V.; Rocha, J. *Solid State Nucl. Magn. Reson.* **2002**, *22*, 501.
(25) Broach, R. W.; Wilson, S. T.; Kirchner, R. M. In *Proceedings of the 12th International Zeolite Conference*; Treacy, M. M. J., Marcus, B. C., Bisher, M. E., Higgens, J. B., Eds.; Materials Research Society: Warrendale PA, 1999; Vol. III, p 1715.
(26) Broach, R. W.; Wilson, S. T.; Kirchner, R. M. *Microporous Mesoporous Mater.* **2003**, *57*, 211.
(27) Zibrowius, B.; Lohse, U.; Richter-Mendau, J. *J. Chem. Soc., Faraday Trans.* **1991**, *87*, 1433.
(28) Brown, S. P.; Wimperis, S. *J. Magn. Reson.* **1997**, *128*, 42.
(29) Kwak, H. T.; Gan, Z. *J. Magn. Reson.* **2003**, *164*, 369.
(30) Ashbrook, S. E.; Wimperis, S. *J. Magn. Reson.* **2002**, *156*, 269.
(31) Ashbrook, S. E.; Wimperis, *Prog. NMR Spectrosc.* **2004**, *45*, 53.

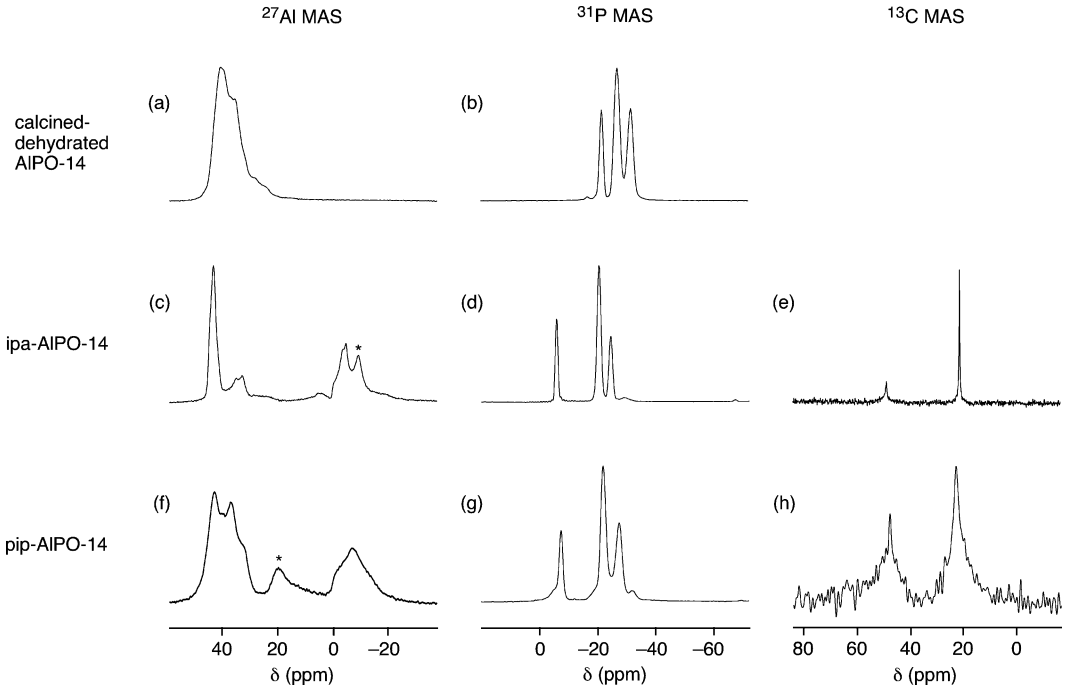

Figure 1. ^{27}Al, ^{31}P, and ^{13}C MAS NMR spectra of calcined-dehydrated AlPO-14, isopropylamine-templated AlPO-14 ("ipa-AlPO-14"), and piperidine-templated AlPO-14 ("pip-AlPO-14"). Spectra are the result of averaging (a−d, f, g) 8, (e) 640, or (h) 320 transients with a relaxation interval of (a, c, f) 0.5 s, (b, d, g) 120 s, (e) 20 s, or (h) 360 s. The MAS rate was 10 kHz. ^{27}Al resonances arising from impurities are indicated by ∗. The ^{13}C MAS spectra were recorded with high-power ^{1}H decoupling.

are reported in parts per million relative to 1 M $Al(NO_3)_3$ (for ^{27}Al), 85% H_3PO_4 (for ^{31}P), or TMS (for ^{13}C). In two-dimensional MQMAS and STMAS experiments, the δ_1 and δ_2 chemical shift scales were calculated and the peaks analyzed as described in ref 31.

Results and General Discussion

The structure of ipa-AlPO-14 has been determined by powder X-ray diffraction[25,26] and has been confirmed by a number of NMR studies.[22−24] The space group is $P\bar{1}$ triclinic with a center of inversion. The unit cell composition corresponds to $Al_8P_8O_{32}(OH)_2{\cdot}(C_3H_{10}N)_2(H_2O)_2$, and there are four ($n = 1-4$) crystallographically distinct phosphorus and aluminum sites, P*n* and Al*n*, respectively. Each crystallographically unique P*n* and Al*n* site has a symmetry equivalent site, P*n*′ and Al*n*′, in the unit cell. The P atoms are tetrahedrally coordinated with framework O atoms. The Al atoms are found in four- (Al2 and Al3), five- (Al1), and six-fold coordination (Al4). Each Al site is coordinated by at least four framework O atoms, while Al1 is additionally coordinated by O9 of an OH^- group. Al4 is coordinated by two additional O atoms, O9 and O9′, of the two OH^- groups of the unit cell. The framework is built up of alternating AlO_x and PO_4 units forming eight-ring channels, where the protonated template cations and additional water molecules are found. In the unit cell, there are two protonated isopropylamine ions and two molecules of water. The exact structure of pip-AlPO-14 remains to be determined, but it has been suggested[27] that it might have the same framework structure as ipa-AlPO-14, with the unit cell having a composition of either $Al_8P_8O_{32}(OH)_2{\cdot}(C_5H_{12}N)(H_3O)(H_2O)$ or $Al_8P_8O_{32}(OH)_2{\cdot}(C_5H_{12}N)_2$. The ^{27}Al MQMAS NMR study, presented below, provides further evidence for the similarity of the ipa- and pip-AlPO-14 framework structures. Calcination of either the ipa- or pip-AlPO-14 materials results in the removal of all template and water molecules to form calcined-dehydrated AlPO-14. The unit cell of calcined AlPO-14 has $P\bar{1}$ space group and has composition $Al_8P_8O_{32}$, with four crystallographically unique four-coordinate P and Al sites.[25,26]

Figure 1a shows the ^{27}Al MAS NMR spectrum of calcined-dehydrated AlPO-14. The ^{27}Al signal intensity is concentrated in a broad peak centered at $\delta \approx 40$ ppm and corresponds to the four four-coordinate Al sites expected from the crystal structure. Some fine structure is present, but the individual second-order quadrupolar broadened ^{27}Al resonances are not resolved. The ^{31}P MAS spectrum in Figure 1b shows three significant peaks at chemical shifts of −21.4, −26.7, and −31.5 ppm with relative intensities of 1:2:1, respectively. An additional, very low-intensity ^{31}P resonance at −18.5 ppm probably arises from an impurity (this and other minor impurity phases mentioned below are not observed in the X-ray diffraction and hence cannot be identified). In analogy with the work in ref 24, it can be assumed that the ^{31}P resonance at −26.7 ppm consists of two overlapping resonances corresponding to two distinct P sites.

The ^{27}Al, ^{31}P, and ^{13}C MAS NMR spectra of ipa-AlPO-14 are shown in Figure 1c−e, respectively. The four-, five-, and six-coordinate Al sites expected from the crystal structure are evident in the ^{27}Al MAS spectrum in Figure 1c. The narrow ^{27}Al resonance at ∼45 ppm and the broader resonance at ∼35 ppm correspond to the two four-coordinate Al sites, the very broad, low-intensity feature lying between 0 and 20 ppm corresponds to the five-coordinate Al site, while the ^{27}Al resonance at ∼ −5 ppm corresponds to six-coordinate Al. The resonance at ∼ −10 ppm in Figure 1c (indicated by ∗) is due to an impurity. In the ^{31}P MAS NMR spectrum in Figure 1d, three significant peaks are observed at chemical shifts of −5.4, −20.2, and −24.3 ppm with relative intensities of 1:2:1. An additional, low-intensity peak at −28 ppm is perhaps due to

the presence of an impurity. It has been demonstrated in ref 14 that high-power {^{27}Al/^{1}H} decoupling narrows the linewidth of the ^{31}P resonance at −20.2 ppm in Figure 1d and results in the resolution of two, otherwise overlapping, ^{31}P resonances. The ^{13}C MAS NMR spectrum in Figure 1e consists of peaks at 48.5 and 21.4 ppm.

The ^{27}Al, ^{31}P, and ^{13}C MAS NMR spectra of pip-AlPO-14 are shown in Figure 1f−h, respectively, and may be interpreted in a manner similar to those of ipa-AlPO-14. The ^{27}Al resonance at ∼20 ppm in Figure 1f (indicated by ∗) is due to an impurity. In the ^{31}P MAS NMR spectrum in Figure 1g, three significant peaks are observed at chemical shifts of −7.1, −21.6, and −27.2 ppm with relative intensities of 1:2:1. Additional, low-intensity peaks at −7, −19, and −33 ppm may be ascribed to impurities. The two peaks observed at 47.7 and 23.1 ppm in the ^{13}C MAS NMR spectrum in Figure 1h are very broad compared with those in the ipa-AlPO-14 spectrum in Figure 1e, possibly indicating a difference in dynamic behavior between the two template molecules. The ^{13}C chemical shifts and those of ipa-AlPO-14 in Figure 1e confirm that the amine template molecules are protonated, thus balancing the negative charge of the hydroxyl group in the framework.

In the course of recording the spectra in Figure 1, it was observed that the spin−lattice (T_1) relaxation rates of the ^{31}P nuclei in calcined-dehydrated AlPO-14 were considerably faster (T_1 = 0.7−1.0 s for the most rapid relaxing component of the multiexponential recovery) than those in ipa- and pip-AlPO-14 (T_1 = 48 s). The most likely reason is the presence of (paramagnetic) O_2 molecules in the channels of calcined AlPO-14. To confirm this, calcination of ipa-AlPO-14 was carried out under a N_2 atmosphere, and significantly decreased ^{31}P spin−lattice relaxation rates were observed (T_1 = 4.5−5.0 s for the most rapid relaxing component of the multiexponential recovery) compared with calcination in air. Similar effects of molecular oxygen on relaxation rate constants in microporous materials have been reported previously.[32−34]

Figure 2 shows the two-dimensional ^{27}Al MQMAS and STMAS spectra and corresponding isotropic projections of both calcined-dehydrated AlPO-14 and ipa-AlPO-14. The ^{27}Al MQMAS and STMAS NMR spectra of calcined AlPO-14 are shown in Figure 2a,b, respectively. Four resonances corresponding to the four crystallographically distinct Al sites are resolved in each spectrum. However, these peaks have not yet been assigned to the crystallographic sites. The ^{27}Al chemical shift and quadrupolar parameters obtained from ref 35 are given in Table 1, where they are labeled Al$^{(IVa-d)}$ in order of decreasing δ_1 shift of the resonances in Figure 2a,b to which they correspond. The resonances in the isotropic projection of the STMAS spectrum in Figure 2f are very slightly broader than those in the isotropic projection of the MQMAS spectrum in Figure 2e. This is most probably the result of a small misset (∼0.003°) of the spinning angle in the NMR probehead (the STMAS experiment is more sensitive to such a misset than the MQMAS experiment[20,30,31]). The ^{27}Al STMAS spectrum in Figure 2b also contains a central-transition autocorrelation peak and a peak arising from the correlation of the $m_I = +1/2 \leftrightarrow -1/2$ central transition and the $m_I = \pm 5/2 \leftrightarrow \pm 3/2$ outer satellite transitions, as indicated on the spectrum. Apart from these trivial

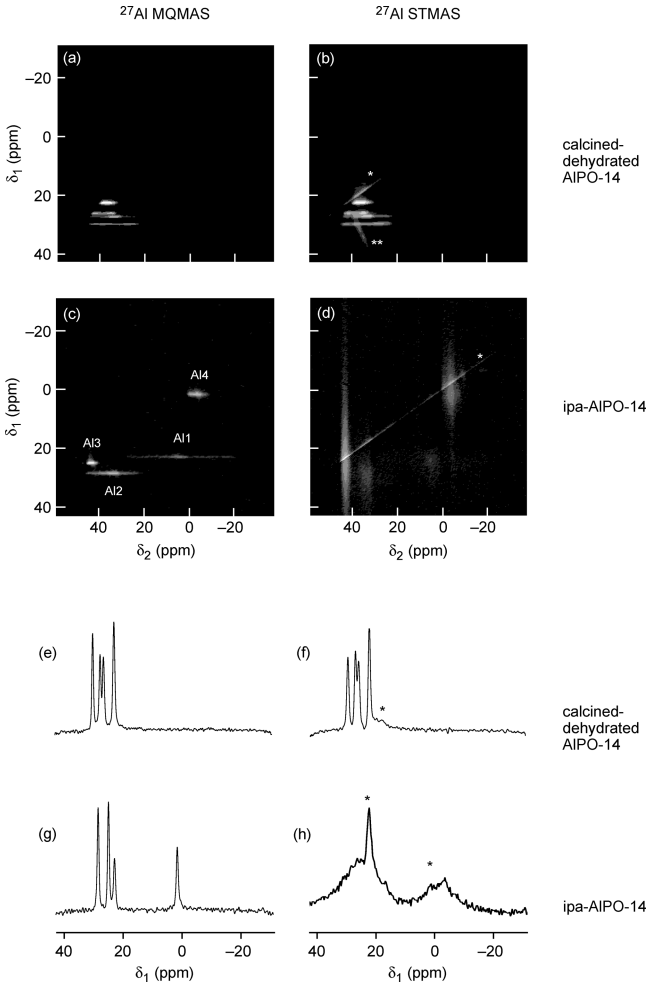

Figure 2. (a−d) Two-dimensional ^{27}Al MQMAS (triple-quantum) and STMAS NMR spectra of calcined-dehydrated AlPO-14 and ipa-AlPO-14 and (e−h) the corresponding isotropic projections. Two-dimensional spectra are the result of averaging 96 transients for each of (a, b) 256 or (c, d) 360 t_1 increments of 64.58 μs, with a relaxation interval of 0.5 s. The MAS rate was 20 kHz. In the STMAS spectra, the central-transition autocorrelation peak and its contribution to the isotropic projection is indicated by ∗, while an outer satellite-transition correlation peak is indicated by ∗∗.

Table 1. Isotropic ^{27}Al Chemical Shifts (δ_{CS}) and Quadrupolar Parameters (coupling constant C_Q and asymmetry η) for the Al Sites in Calcined-Dehydrated AlPO-14 (taken from ref 35), ipa-AlPO-14 (taken from ref 22 and confirmed by analysis of ^{27}Al MQMAS spectrum in Figure 2c), and in pip-AlPO-14 (extracted from ^{27}Al MQMAS spectrum in Figure 5a)

Al site	δ_{CS} (ppm)	C_Q/MHz	η
	calcined-dehydrated AlPO-14		
Al$^{(IVa)}$	45	4.9	0.3
Al$^{(IVb)}$	43	4.0	0.8
Al$^{(IVc)}$	43	3.4	0.2
Al$^{(IVd)}$	38	2.5	0.6
	ipa-AlPO-14		
Al1	27	5.6	1.0
Al2	44	4.1	0.8
Al3	43	1.7	0.6
Al4	−1	2.6	0.7
	pip-AlPO-14		
Al$^{(V)}$	28	5.9	0.5
Al$^{(IVa)}$	46	2.9	0.8
Al$^{(IVb)}$	39	3.2	0.1
Al$^{(VI)}$	−1	3.3	0.9

(32) Accardi, R. J.; Lobo, R. F. *Microporous Mesoporous Mater.* **2000**, *40*, 25.
(33) Accardi, R. J.; Lobo, R. F.; Kalwei, M. *J. Phys. Chem. B* **2001**, *105*, 5883.
(34) Liu, H.; Grey, C. P. *Microporous Mesoporous Mater.* **2002**, *53*, 109.
(35) Amoureux, J. P.; Huguenard, C.; Engelke, F.; Taulelle, F. *Chem. Phys. Lett.* **2002**, *356*, 497.

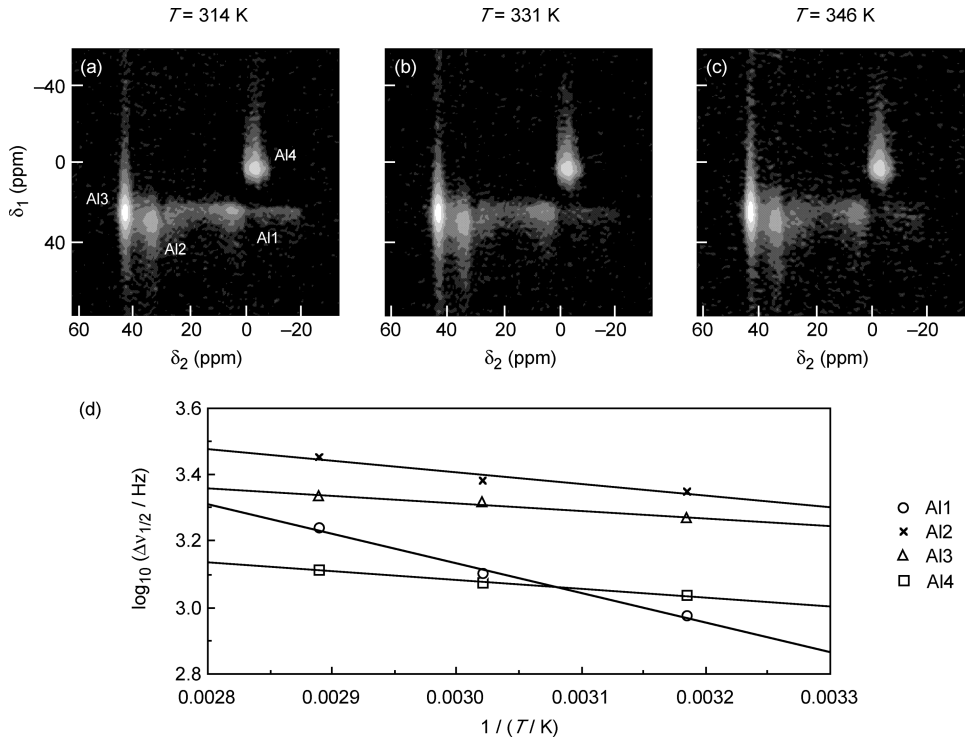

Figure 3. (a−c) Two-dimensional ^{27}Al DQF-STMAS NMR spectra of ipa-AlPO-14 recorded at temperatures of 314, 331, and 346 K. Spectra are the result of averaging 1024 transients for each of 48 t_1 increments of 64.58 μs, with a relaxation interval of 0.5 s. The MAS rate was 20 kHz. (d) Log_{10} of the experimental isotropic linewidth, $\Delta\nu_{1/2}$, plotted as a function of $1/T$ for the four Al sites.

differences, the two two-dimensional spectra in Figure 2a,b and the two isotropic projections in Figure 2e,f are essentially identical.

The ^{27}Al MQMAS and STMAS NMR spectra of ipa-AlPO-14 are shown in Figure 2c,d, respectively. The four ridge lineshapes in the ^{27}Al MQMAS spectrum correspond to the four well-resolved resonances in the isotropic projection in Figure 2g. The ^{27}Al chemical shift and quadrupolar parameters obtained from ref 22 (and confirmed in this study) are given in Table 1, where they have been assigned according to ref 24. In contrast to the MQMAS spectrum, the ^{27}Al STMAS spectrum of ipa-AlPO-14 in Figure 2d and its isotropic projection in Figure 2h reveal four ^{27}Al resonances that are significantly broadened in the δ_1 dimension. It will be shown in the next section that the cause of this broadening is a dynamics-driven modulation of the ^{27}Al quadrupolar interaction on the microsecond timescale.

One of the characteristic features of motional broadening is its temperature dependence. The ^{27}Al DQF-STMAS NMR spectra of ipa-AlPO-14 recorded at 314, 331, and 346 K are shown in Figure 3a−c, respectively. The DQF-STMAS method, rather than the basic STMAS experiment, is used here because the resulting spectra are free of the central-transition autocorrelation ridge, which is not subject to strong motional broadening and thus makes measurement of linewidths in the isotropic projection difficult (e.g., see Figure 2h). The linewidth changes in the δ_1 (isotropic) dimension are small but significant with all four Al sites exhibiting an increase in linewidth as T increases. In Figure 3d, the logarithm of the experimental full linewidth at half-height in the isotropic projection ($\Delta\nu_{1/2}$) is plotted against $1/T$ for the four Al sites in ipa-AlPO-14.

Both water and isopropylamine molecules occur in the cages of the ipa-AlPO-14 structure. In an attempt to distinguish between these two potential sources of dynamic behavior in the solid, the water molecules were removed from ipa-AlPO-14 by heating at 200 °C for 1 h. The ^{27}Al and ^{31}P MAS NMR spectra of this material are shown in Figure 4a,b, respectively. The spectrum in Figure 4a suggests the presence of four-, five-, and six-coordinate Al sites. Four sharp ^{31}P resonances at chemical shifts of −7.8, −20.5, −21.5, and −24.7 ppm, and one considerably broader resonance at −31 ppm, are observed in Figure 4b. The broad ^{31}P resonance is observed in the chemical shift region of the calcined AlPO-14, suggesting that the template molecule was removed from a proportion of AlPO-14 during the heating process. The ^{27}Al MQMAS NMR spectrum of dehydrated ipa-AlPO-14 in Figure 4c displays four ridge-like lineshapes, while the resonance centered on ∼37 ppm in the δ_2 dimension (indicated by ∗) is assigned to calcined AlPO-14. Motional broadening of all four peaks is evident in the δ_1 dimension of the ^{27}Al STMAS NMR spectrum of dehydrated ipa-AlPO-14 in Figure 4d.

The ^{27}Al MQMAS spectrum of pip-AlPO-14 in Figure 5a provides strong evidence for a basic similarity in the framework structure of ipa- and pip-AlPO-14. The spectrum displays four ridge-like lineshapes corresponding to the four (presumed) crystallographically distinct Al sites. The isotropic projection of the MQMAS spectrum shows that the ^{27}Al resonances are slightly broader than those observed for ipa-AlPO-14 in Figure 2c, which might be the result of a degree of structural disorder. The isotropic chemical shifts and the quadrupolar parameters for all Al sites, extracted from the spectrum in Figure 5a, are given in Table 1. The ^{27}Al resonances with $\delta_{CS} = -1$ ppm and $\delta_{CS} = 28$ ppm correspond to six- and five-coordinate Al sites (designated $Al^{(VI)}$ and $Al^{(V)}$ in Figure 5a and Table 1), respectively. The two other resonances with $\delta_{CS} = 46$ ppm and

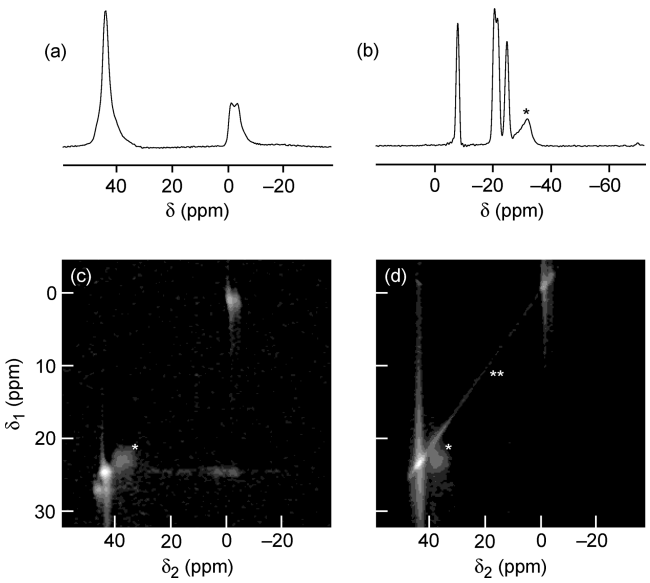

Figure 4. (a) ^{27}Al and (b) ^{31}P MAS NMR spectra and two-dimensional (c) ^{27}Al MQMAS and (d) ^{27}Al STMAS NMR spectra of dehydrated ipa-AlPO-14. Spectra (a, b) are the result of averaging 8 transients with a relaxation interval of (a) 0.5 s and (b) 60 s. Spectra (c, d) are the result of averaging (c) 480 and (d) 320 transients for each of 128 t_1 increments of 129.17 μs, with a relaxation interval of 0.5 s. The MAS rate was 10 kHz. Peaks believed to originate from a small amount of calcined-dehydrated AlPO-14 are indicated by $*$, while the central-transition autocorrelation peak in (d) is indicated by $**$.

$\delta_{CS} = 39$ ppm correspond to four-coordinate Al sites (designated $Al^{(IVa)}$ and $Al^{(IVb)}$, respectively, in Figure 5a and Table 1). In view of their similar framework structures, it might be expected that NMR spectra of ipa-AlPO-14 and pip-AlPO-14 would yield similar ^{27}Al isotropic chemical shifts and quadrupolar parameters. Although it is found here that the five- and six-coordinate Al sites of ipa- and pip-AlPO-14 have very similar δ_{CS} and C_Q values, for the four-coordinate Al sites, the ^{27}Al δ_{CS} and C_Q values differ significantly, possibly indicating that a change in the local Al environment has occurred at these sites. Similarly, significant differences in asymmetry parameter, η, may also indicate a change in the local Al environment, for example, between the five-coordinate site in ipa-AlPO-14 ($\eta = 1.0$) and pip-AlPO-14 ($\eta = 0.5$).

The ^{27}Al DQF-STMAS NMR spectra of pip-AlPO-14 recorded at 314, 331, and 346 K are shown in Figure 5b−d, respectively, and show motionally broadened peaks. At 314 K, the ^{27}Al resonances corresponding to five- and six-coordinate Al are barely observable, owing to very large motional broadenings in the δ_1 dimension. At 346 K, the motional broadening of the two four-coordinate Al sites is larger than that at 314 K, while the ^{27}Al resonance of the five-coordinate Al site is narrowed sufficiently such that it is now clearly observable. The ^{27}Al resonance corresponding to the six-coordinate Al site is just observable at 346 K, but it was not possible to measure the δ_1 linewidth accurately. In Figure 5e, the logarithm of the experimental full linewidth at half-height in the isotropic projection ($\Delta\nu_{1/2}$) is plotted against $1/T$ for the two four-coordinate and the five-coordinate Al sites in pip-AlPO-14.

Motional Broadening Discussion

As we have discussed in ref 21, the cause of the strong line-broadening in the δ_1 dimension of STMAS NMR spectra is dynamics within the solid. In the STMAS experiment, MAS is used to remove the inhomogeneous first-order quadrupolar broadening from the $m_I = \pm 3/2 \leftrightarrow \pm 1/2$ satellite transitions during the t_1 evolution period. Typically, the magnitude of this first-order broadening is ~1 MHz, and hence the MAS rate will be much less than the static linewidth. Therefore, the t_1 time-domain data will consist of a series of sharp rotary echoes, and the corresponding spectrum will consist of a series of spinning sidebands in the δ_1 dimension which are intentionally aliased onto the centerband ("rotor-synchronized" acquisition) so that only a single resonance is observed. A motion-induced change in the quadrupole tensor during the MAS rotor period will interfere with the formation of the echo at end of the rotor period, thus greatly reducing its intensity and producing a very significant homogeneous motional broadening of the spinning sidebands.

In contrast, the MQMAS method correlates transitions that have no first-order quadrupolar broadening, that is, typically triple-quantum coherence $m_I = +3/2 \leftrightarrow -3/2$ and the single-quantum central transition $m_I = +1/2 \leftrightarrow -1/2$. For these transitions, the MAS rate will exceed the static linewidth, and, as a result, they will be strongly narrowed by MAS, that is, averaging will take place continuously throughout a rotor period and the t_1 time-domain data will not exhibit pronounced rotary echoes. In this case, a dynamics-driven modulation of the quadrupole tensor during a rotor period will not result in strong motional line-broadening.

In ref 21, we introduced a simple mathematical model for the motional broadening observed under MAS. The rotary echoes formed during MAS are modeled as simple Hahn echoes, and an exact average Liouvillian operator can be calculated that describes the time evolution across one echo period, with the (real) eigenvalues of this operator corresponding to the homogeneous decay rate constant, R, in the presence of dynamics:

$$R = -\frac{1}{\tau_{MAS}}\ln\{A(B \pm C)\} + R_0 \quad (1)$$

where

$$A = \frac{\exp(-k\tau_{MAS})}{4q^2\exp(-q\tau_{MAS})} \quad (2a)$$

$$B = 2k^2\{1 + \exp(-2q\tau_{MAS})\} - (2\pi\Delta\nu_{jump})^2\exp(-q\tau_{MAS}) \quad (2b)$$

$$C = 2k\{\exp(-q\tau_{MAS}) - 1\} \times \sqrt{k^2\{1 + \exp(-q\tau_{MAS})\}^2 - (2\pi\Delta\nu_{jump})^2\exp(-q\tau_{MAS})} \quad (2c)$$

with

$$q = \sqrt{k^2 - (\pi\Delta\nu_{jump})^2} \quad (2d)$$

The parameters in the model are the first-order rate constant, k (in s^{-1}), for the motional process (assuming dynamic exchange between two sites with identical populations), the size of the jump in resonance frequency, $\Delta\nu_{jump}$ (in Hz), that occurs when the motion-induced change in the quadrupole tensor takes place, the rotor period, $\tau_{MAS} = 1/\nu_{MAS}$, where ν_{MAS} is the MAS rate in Hz, and the resonance half-linewidth at half-height in the absence of motion, R_0 (in s^{-1}). The ^{27}Al quadrupolar coupling

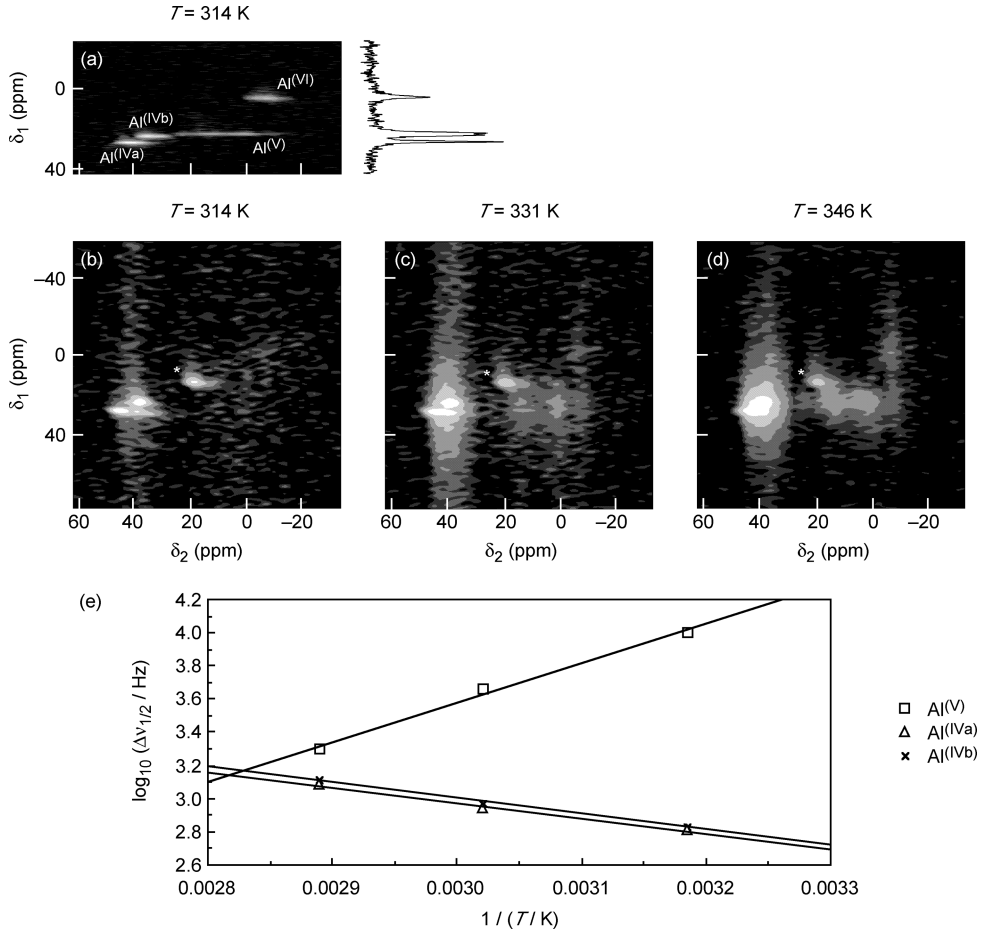

Figure 5. (a) Two-dimensional ^{27}Al MQMAS NMR spectrum of pip-AlPO-14 recorded at 314 K and (b−d) two-dimensional ^{27}Al DQF-STMAS NMR spectra recorded at 314, 331, and 346 K. Spectra are the result of averaging (a) 960 and (b−d) 2048 transients for each of (a) 240 and (b−d) 48 t_1 increments of 64.58 μs, with a recycle interval of 0.5 s. The MAS rate was 20 kHz. An ^{27}Al resonance arising from an impurity is indicated by ∗. (e) Log_{10} of the experimental isotropic linewidth, $\Delta\nu_{1/2}$, plotted as a function of $1/T$ for the three Al sites that can be measured.

constants for ipa-AlPO-14 and pip-AlPO-14 in Table 1 range up to $C_Q \approx 6$ MHz in magnitude, and therefore it is appropriate to explore motional broadening for frequency jumps, $\Delta\nu_{\mathrm{jump}}$, ranging from ∼5 kHz (appropriate for a triple-quantum transition or central transition broadened only by the second-order quadrupolar interaction, chemical shift anisotropy, and dipolar couplings) up to ∼500 kHz (since $\nu_Q^{\mathrm{PAS}} = 3C_Q/40$ for spin $I = 5/2$) for satellite transitions broadened by the first-order quadrupolar interaction. Using this model, a $\log_{10}-\log_{10}$ plot of the motionally broadened linewidth R/π (full-width at half-height in Hz) against the rate constant k is shown in Figure 6 for a range of $\Delta\nu_{\mathrm{jump}}$ values between 5 and 500 kHz, assuming $\nu_{\mathrm{MAS}} = 20$ kHz and $R_0/\pi = 50$ Hz. In interpreting this plot, it should be remembered that the model is crude and breaks down for k values greater than $\sim 10^9$ s^{-1}, where the dynamics become fast enough to induce $\Delta m_I = \pm 1$ and ± 2 transitions, leading to additional motional broadening.

The quadrupole interaction tensor **Q** is given by

$$\mathbf{Q} = eQ\mathbf{V}/2I(2I-1)\hbar \qquad (3)$$

where Q is the nuclear quadrupole moment, and e is the elementary charge. Hence, **Q** is proportional to the electric field gradient tensor **V**. The tensor **Q** is usually parametrized by a coupling constant $C_Q = eQV_{zz}/h$ and an asymmetry $\eta = (V_{xx} - V_{yy})/V_{zz}$, where the V_{ii} are the principal axes of the field gradient

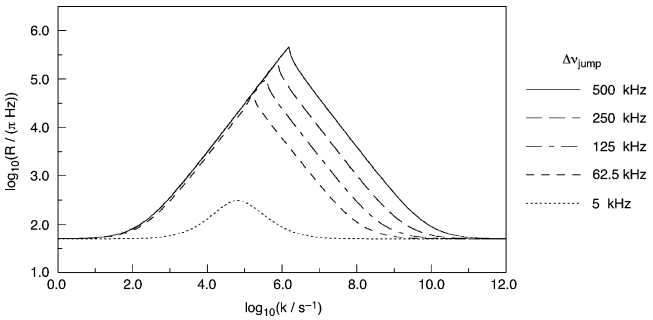

Figure 6. Log_{10} of the theoretical linewidth R/π (full-width at half-height in Hz) as a function of $\log_{10}$ of the rate constant k calculated using the model of motional broadening under MAS described in ref 21 and eqs 1 and 2. The MAS rate was 20 kHz, and the inherent linewidth R_0/π (full-width at half-height) was 50 Hz.

tensor **V** (defined such that $|V_{zz}| \geq |V_{yy}| \geq |V_{xx}|$), and these are the quadrupolar parameters we have used, for example, in Table 1. A motion-induced change or "jump" in the magnitude or direction of the ^{27}Al quadrupolar interaction is therefore caused by a corresponding jump in the magnitude or direction of the electric field gradient around the ^{27}Al nucleus. Note, however, that this change in the EFG tensor does not necessarily have to be brought about by any motion of the Al atom itself relative to other Al or P sites; instead, the EFG tensor can be modulated by dynamics in the immediate environment of the

Al atom, for example, by motion of some nearby atom or molecular fragment.

The ^{27}Al MQMAS and STMAS spectra of calcined-dehydrated AlPO-14 in Figure 2a,b and their isotropic projections in Figure 2e,f are essentially identical. Inspection of Figure 6 shows that there is no significant motion in calcined AlPO-14 that modulates any of the ^{27}Al EFG tensors and that has a rate constant between $k \sim 10^3$ and 10^9 s^{-1}, or on a timescale ($\tau = 1/k$) between 0.001 and 1000 μs. Within these timescale limits, therefore, calcined-dehydrated AlPO-14 can be described as a rigid framework structure with no dynamics.

In contrast, all four sites in the ^{27}Al STMAS spectrum of ipa-AlPO-14 in Figure 2d and its isotropic projection in Figure 2h exhibit significant motional broadening (on the order of 10^3 Hz) in the δ_1 dimension when compared with the MQMAS spectrum in Figure 2c. Therefore, according to Figure 6, there must be significant modulations of all four ^{27}Al EFG tensors, and these must be on timescales between 0.01 and 1000 μs. If the motional broadening is the dominant line-broadening mechanism, the Arrhenius-type plots of $\log_{10}(\Delta\nu_{1/2}/\text{Hz})$ against $1/T$ in Figure 3d should yield gradients of $\pm\Delta E_A/(2.303N_A k_B)$, where ΔE_A is the activation energy, N_A is the Avogadro constant, and k_B is the Boltzmann constant. The activation energies found by this method were 17 kJ mol^{-1} for Al1, 7 kJ mol^{-1} for Al2, 4 kJ mol^{-1} for Al3, and 5 kJ mol^{-1} for Al4. These are all much lower than would be found for a bond-breaking process and are typical of values expected for molecular conformational change. If there was a single motional process occurring in ipa-AlPO-14 and modulating the EFG tensors at all four Al sites, it would be expected that the activation energies found would be the same for all four sites. Instead, we find that the activation energy for the motion at Al1 differs significantly, indicating either that a second, distinct motional process is at work at Al1 or that there are multiple motional processes occurring in the solid, each with a different degree of influence at each Al sites. In this latter case, the apparently straight lines in Figure 3d would be an artifact of the relatively small temperature range accessible to standard MAS probeheads.

It seems unlikely that the motional processes responsible for the observed line-broadening originate entirely within the ipa-AlPO-14 framework. The most likely sources of dynamics in ipa-AlPO-14 are the isopropylamine template and water molecules occluded within the framework. It may be envisaged either that the framework remains rigid and that the motion of the guest molecules alone modulates the ^{27}Al EFG tensors or, more likely, that motion of the guest molecules results in a sympathetic flexing of the framework, with the latter providing a more direct mechanism for modulation of the ^{27}Al EFG tensors. The results in Figure 4 show that even in dehydrated ipa-AlPO-14, where water molecules are absent from the cages, motional broadening of the ^{27}Al peaks is still observed. Similarly, ^{27}Al STMAS spectra of calcined and then rehydrated AlPO-14 exhibit significant motional broadening (results not shown), although comparison with the MQMAS spectrum reveals that some static disorder is also present.[36] Therefore, it appears that both the isopropylamine and water molecules in the ipa-AlPO-14 cages contribute to the dynamics observable in the ^{27}Al STMAS spectra.

In contrast to ipa-AlPO-14, the exact structure of pip-AlPO-14 is yet to be determined, although the NMR spectra shown here suggest that the framework structures are similar. All four resonances in the ^{27}Al STMAS spectra of pip-AlPO-14 in Figure 5b−d exhibit significant broadenings (of the order of 10^3-10^4 Hz) in the δ_1 dimension when compared with the MQMAS spectrum in Figure 5a, corresponding to motions with timescales between 0.01 and 1000 μs. The Arrhenius-type plots of $\log_{10}(\Delta\nu_{1/2})$ against $1/T$ in Figure 5e yield activation energies of 45 kJ mol^{-1} for Al$^{(V)}$, 18 kJ mol^{-1} for Al$^{(IVa)}$, and 18 kJ mol^{-1} for Al$^{(IVb)}$. The activation energy for Al$^{(VI)}$ cannot be determined but is clearly similar to or larger than that of Al$^{(V)}$. Although larger on average than those found in ipa-AlPO-14, the activation energies for pip-AlPO-14 are still of a magnitude that is indicative of conformational change.

It is evident that the variable-temperature ^{27}Al STMAS results in Figures 3 and 5 are not explicable under the assumption of there being a single motional process in the solid with a well-defined first-order rate constant k, with both the signs and magnitudes of the gradients in Figures 3d and 5b differing from Al site to Al site in a way that is not consistent with the simple model in Figure 6. They therefore appear to indicate that the dynamics in ipa-AlPO-14 and pip-AlPO-14 are complex, and this view is further supported by the apparent involvement of both template and water molecules. The larger activation energies in Figure 5e, the much broader ^{13}C resonances in Figure 1h, and the slightly broadened isotropic ^{27}Al MQMAS spectrum in Figure 5a all suggest that the dynamics in pip-AlPO-14 are slower than those in ipa-AlPO-14 and that any conformational process is more restricted. This is consistent with chemical intuition based on the relative size of the isopropylamine and piperidine molecules and their corresponding degrees of motional freedom, with the latter being a more voluminous molecule with a rigid six-membered ring structure.

Conclusions

The sensitivity of isotropic STMAS NMR linewidths to dynamics on the microsecond timescale, previously only reported in an ^{17}O NMR study of dense silicates, has been used here in an ^{27}Al NMR study of dynamics in three forms of AlPO-14. Although calcined-dehydrated AlPO-14 appears to be a rigid framework structure, the extent of motion in the two as-synthesized forms revealed by the novel methodology is surprising, with clear evidence for significant dynamics on the microsecond timescale in the immediate environments of all four Al sites in each material. In diffraction-based techniques, information on such dynamics is contained in a highly averaged form within the atomic temperature factors, and these are difficult to refine from powder data (which are usually the only diffraction data available for microporous solids), with severe approximations often being made. In view of this and of the ability of our new NMR approach to observe dynamics, therefore, it seems likely that the comparison of isotropic MQMAS and STMAS linewidths for nuclei, such as ^{17}O, ^{23}Na, ^{27}Al, and ^{71}Ga, will become an important technique in the study of host−guest interactions and guest dynamics in framework solids. In the present study, the dynamics in the isopropylamine- and piperidine-templated AlPO-14 appear to be complex, and further work

(36) Yang, H.; Walton, R. I.; Biedasek, S.; Antonijevic, S.; Wimperis, S.; Ramirez-Cuesta, A. J.; Li, J.; Kolesnikov, A. I. *J. Phys. Chem. B* **2005**, *109*, 4464.

involving computer simulation, NMR, and other analytical and spectroscopic techniques will have to be carried out to interpret the wealth of detail presented here.

Acknowledgment. We are grateful to EPSRC (Grant No. GR/N07622) and the Nuffield Foundation for financial support, to Sasol Ltd. for donating the hydrated alumina, and to the Royal Society for awards of a Dorothy Hodgkin Fellowship (to S.E.A.) and a K. C. Wong Fellowship (to H.Y.).

JA057682G